Chemosensors

DOI: 10.1002/anie.201004975

Cubic Mesoporous Graphitic Carbon(IV) Nitride: An All-in-One Chemosensor for Selective Optical Sensing of Metal Ions**

Eun Zoo Lee, Young-Si Jun, Won Hi Hong,* Arne Thomas, and Moonsoo M. Jin*

Carbon nitride is an appealing class of material which can complement carbon in a variety of applications. At ambient conditions a graphitic carbon nitride (g-C_3N_4) is regarded to be the most stable allotrope.[1] Kroke et al. proposed that g-C_3N_4 consists of sheets of ordered tri-s-triazine moieties connected through planar tertiary amino groups stacked in a graphitic fashion.[2] The bulk material synthesis of g-C_3N_4 was attempted by thermal condensation of nitrogen-rich precursors, even though most reactants do not proceed significantly past the polymeric form owing to incomplete condensation or polymerization in the bulk.[3] A higher condensation degree was achieved by carrying out the condensation in molten salts.[4]

Graphitic carbon nitride has recently attracted great interests because of its semiconductor properties, which makes it suitable for photocatalytic applications. The electronic band structure and band gap of g-C_3N_4 depend on the degree of condensation of the material.[5] It was also proposed that the band gap can be tuned to lower or higher values by protonation or synthesis of inclusion complex with metal cations such as Zn^{2+} and Fe^{3+}.[6,7] g-C_3N_4 has been used as a photocatalyst for the production of hydrogen and oxygen from water.[6,8] The introduction of porosity into g-C_3N_4 yields an increase in the accessible surface area of the material. It was also shown that the catalytic and photocatalytic activity of mpg-C_3N_4 ("mesoporous graphitic carbon nitride") greatly improved over that of the bulk material.[9,10]

Optical sensors are molecular receptors whose optical properties change upon binding to specific guests.[11] Optical sensing systems have been intensively investigated for their capability of providing sensitivity and fast and easy detection, biocompatibility, and adaptability to a wide variety of assay conditions.[12] One notable application of optical sensors is in the sensing of metal ions. Especially in industrial areas, large amounts of toxic and carcinogenic metals have been released into the environment, which has strongly raised interest in the biological and environmental monitoring of such compounds.[13] Various optical sensors based on azo-coupled macrocycles, porphyrin, and phenanthroline derivatives have been described for the detection of a wide range of metal ions.[13–15] The Lewis basic site on these molecular receptors provides strong coordination to metal ions while the net electron transfer from chromophore/fluorophore group in the receptor to the complexed metal ions leads to the qualitative and semiquantitative sensing of metal ions. Recent development in mesoporous materials has improved the performance of these sensors through immobilization of receptors, whereby the receptors are attached to a large and accessible surface area and well-defined pores, favorable for high adsorption capacity of chromogenic/fluorescent molecules and efficient transport of analytes and thus low detection limits of below tens of nanomolar concentrations.[14,16] There is, however, still growing demand for more advanced optical sensing system with lower detection limit and faster kinetic response. Considering the properties of present chromogenic/fluorescent receptors, it seems that nanostructured g-C_3N_4 would be a promising alternative. As previously described, the electronic structure of g-C_3N_4 is adjustable by coupling events of protons or metals to the surface. The surface functionalities of g-C_3N_4, that is, $-NH_2$/$-NH-$/$=N-$, are well-characterized ligands exhibiting high adsorption capacity for metal ions through chelation or redox reaction. Finally, an additional supporting material is not necessary because it is possible to tailor its nanostructure by using any kind of silica hard template. In comparison with the systems in which the receptor is supported on a porous material, and thus constitute just a minor part, considering weight and volume fraction of the overall system, in mpg-C_3N_4 the entire material would be composed of the functional, in this case sensing, material, which principally gives rise to very high sensitivity. Such a nanostructuring is also necessary for efficient transport of metal ions to the surface.

Herein, we utilized g-C_3N_4 as an all-in-one chemosensor to detect trace amounts of metal ions in aqueous solutions. For this purpose 3D cubic ($Ia\bar{3}d$) mesoporous g-C_3N_4 (c-mpg-C_3N_4) with high surface area was synthesized for the first time. The electronic properties as well as the surface functionalities of c-mpg-C_3N_4 should make it an efficient optical sensor. Structural characterization of c-mpg-C_3N_4 was carried out by small- and wide-angle X-ray scattering (SAXS and WAXS), transmission electron microscopy (TEM), N_2 sorption, thermogravimetric analysis (TGA), Fourier transform infrared

[*] E. Z. Lee, Dr. Y.-S. Jun, Prof. W. H. Hong
Department of Chemical and Biomolecular Engineering, KAIST
335 Gwahak-ro, Yuseong-gu, Daejeon, 305-701 (Korea)
Fax: (+82) 42-350-3910
E-mail: st9750@kaist.ac.kr
whhong@kaist.ac.kr
Homepage: http://sep.kaist.ac.kr
Prof. A. Thomas
Institut für Chemie, Technische Universität Berlin
Englische Strasse 20, 10587 Berlin (Germany)
E. Z. Lee, Prof. M. M. Jin
Department of Biomedical Engineering
Cornell University, Ithaca, NY 14853 (USA)

[**] This work was supported by a grant from the Genome-based Integrated Bioprocess Project of the Ministry of Science and Technology of Korea and Brain Korea 21 (BK21).

Supporting information for this article is available on the WWW under http://dx.doi.org/10.1002/anie.201004975.

(FTIR) spectroscopy, and elemental analysis. The ligation ability and electronic communication of c-mpg-C_3N_4 with metal ions were investigated by X-ray photoelectron spectroscopy (XPS), optical absorption and photoluminescence spectroscopy, and fluorescence microscopy.

c-mpg-C_3N_4 was prepared by a nanocasting approach using the ordered mesoporous silica KIT-6 as hard template. The two enantiomeric pore channels in KIT-6 were interconnected by hydrothermal treatment at 130 °C and subsequently filled with cyanamide and heated to 550 °C. Removal of the silica with HF resulted in the formation of a g-C_3N_4 replica with 3D cubic ($Ia\bar{3}d$) symmetry, as shown by XRD and TEM measurements (Figures 1 and 2). TGA measurements showed that the silica template was completely removed (Figure S1 in the Supporting Information).

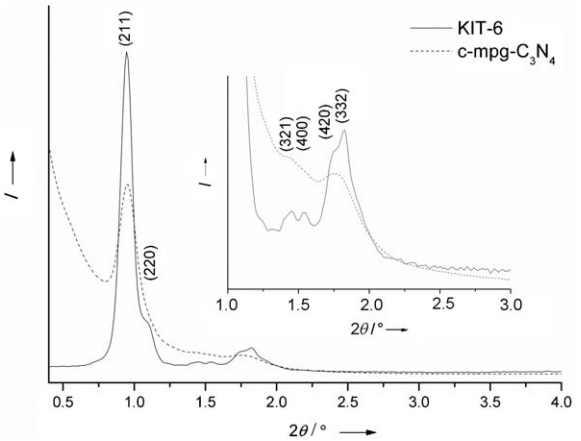

Figure 1. SAXS patterns of 3D cubic ($Ia\bar{3}d$) mesoporous silica KIT-6 and c-mpg-C_3N_4. The inset shows the SAXS patterns in the range from 1 to 3°.

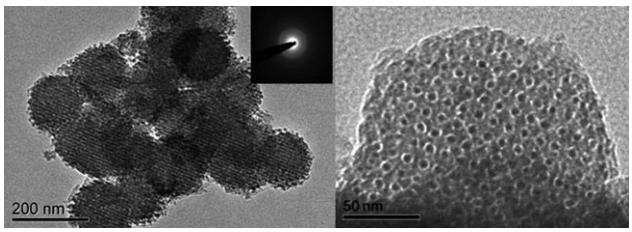

Figure 2. TEM images of c-mpg-C_3N_4 in different directions.

The nitrogen sorption measurements show a type IV isotherm with H_1 hysteresis loop, indicative for a mesoporous material (Figure S2). Brunauer–Emmett–Teller (BET) measurements reveal a surface area of 208 $m^2 g^{-1}$ and a pore volume of 0.4 $cm^3 g^{-1}$ (Table 1). The high degree of condensation without forming texture pores is responsible for lower surface area of c-mpg-C_3N_4 than that of parent KIT-6. The pore size distribution calculated by the Barrett–Joyner–Halenda (BJH) method is centered at 3.6 nm. The absence of additional reflection below $2\theta = 0.7°$ in the XRD pattern and mesopores close to 11 nm in diameter in pore size distribution confirms that it is indeed an exact replica of KIT-6 without structural displacement between two enantiomeric g-C_3N_4 frameworks.[17]

Table 1: Textural properties of g-C_3N_4s and KIT-6.

Material	S_{BET} [$m^2 g^{-1}$][a]	Pore volume [$cm^3 g^{-1}$]	w_{BJH} [nm][b]	a [nm][c]	d (nm)[d]
bulk g-C_3N_4	8	0.1	–	–	–
c-mpg-C_3N_4	208	0.4	3.6	22.7	7.5
KIT-6	606	1.2	9.8	24.3	3.5

[a] BET surface area. [b] w_{BJH} calculated from the adsorption branch of the nitrogen sorption isotherm by the BJH method. [C] XRD unit cell parameter a calculated from the equation $a = \sqrt{6}\, d_{211}$. [d] Wall thickness d estimated from TEM images.

The wall thickness was estimated from TEM images to be about 7.5 nm. Deviation of the wall thickness from the pore size (9.8 nm) of the parent KIT-6 can be explained by the volume decrease of the precursor upon formation of the condensed material during heat treatment (Table 1).[18] However, this contraction results mainly in shrinkage of only the pore walls, as the observed decrease in the lattice parameter from the template (24.3 nm) to its replica (22.7 nm) is insignificant.

The structure of c-mpg-C_3N_4 was further evaluated by WAXS and elemental analysis. The WAXS pattern of c-mpg-C_3N_4 shows an intense peak centered at $2\theta = 27.47°$, corresponding to a typical graphite-like stacking of C_3N_4 layers with an interlayer distances of $d = 0.324$ nm (Figure S3). The XRD pattern of c-mpg-C_3N_4 features the characteristic peaks of the bulk material, while broadening of the peaks and a significant decrease in overall intensities can be attributed to the reduced correlation length introduced by nanostructuring.[9]

Elemental analysis was performed three times on different batches of g-C_3N_4s. An average C/N ratio of 0.68 for c-mpg-C_3N_4 indicates that the organization level is still far from an ideal single crystalline g-C_3N_4 with theoretical C/N ratio of 0.75. The high amount of residual hydrogen (3.1 % for c-mpg-C3N4 compared with 1.9 % for bulk g-C_3N_4) shows the introduction of a high surface area, which is terminated by uncondensed amine groups, also seen by FTIR analysis. The FTIR spectra show the characteristic bands of tri-s-triazine based g-C_3N_4 (Figure S4). Strong bands in the 1200–1600 cm^{-1} region are attributed to the stretching vibrations of aromatic CN heterocycles.[4] The absorption at 803 cm^{-1} is characteristic of out-of-plane bending modes of tri-s-triazine. Additional broad bands corresponding to N–H stretching vibration modes were observed in the 3000–3500 cm^{-1} region, which indicates the presence of primary and secondary amines probably in the form of C–NH_2 and C–NH–C, respectively.[19]

c-mpg-C_3N_4 was added to metal nitrate solutions in tris-HCl buffer (pH 7.4; tris = tris(hydroxymethyl)aminomethane) and mixed for 1 h to form metal ion–c-mpg-C_3N_4 complexes. The effect of metal ion coordination on the electronic structure of c-mpg-C_3N_4 was seen in photoluminescence (PL) and UV/vis spectra. The PL spectrum of pure c-mpg-C_3N_4 shows a broad peak at $\lambda = 455$ nm with an excitation wavelength of $\lambda = 375$ nm (Figure S5). Electron

localization on the surface terminal sites is seen by the suppression of PL intensity relative to that of bulk g-C_3N_4.[20] Figure 3a shows the percentage PL quenching of c-mpg-C_3N_4 in the presence of Zn^{2+}, Hg^{2+}, Pb^{2+}, Co^{2+}, Mg^{2+}, Cu^{2+}, Fe^{3+}, Mn^{2+}, Cd^{2+}, and Ni^{2+}. It was found that c-mpg-C_3N_4 exhibits excellent selectivity for Cu^{2+} over other metal ions. A sample of 10 mg of c-mpg-C_3N_4 lost almost all PL intensity (98%) with 10 mL of 1 mM Cu^{2+} solution, and no interference from the coexistence of other metal ions was observed (white bars). The PL spectrum of c-mpg-C_3N_4 was gradually quenched with increasing Cu^{2+} concentration from 100 nM to 1 mM (Figure S6). In contrast, bulk g-C_3N_4 shows different results in PL quenching, that is, just a low response to the metal ions, demonstrating that the nanostructuring is indeed essential for the electronic communication between the metal ion and the adsorbent. In addition to Cu^{2+}, also Co^{2+} and Pb^{2+} show PL quenching of 30 and 26%, respectively. We attribute this quenching to the redox potentials of Cu^{2+}, Co^{2+}, and Pb^{2+} lying between the electronic band structures of c-mpg-C_3N_4, which is favorable for photoinduced electron transfer (PET).

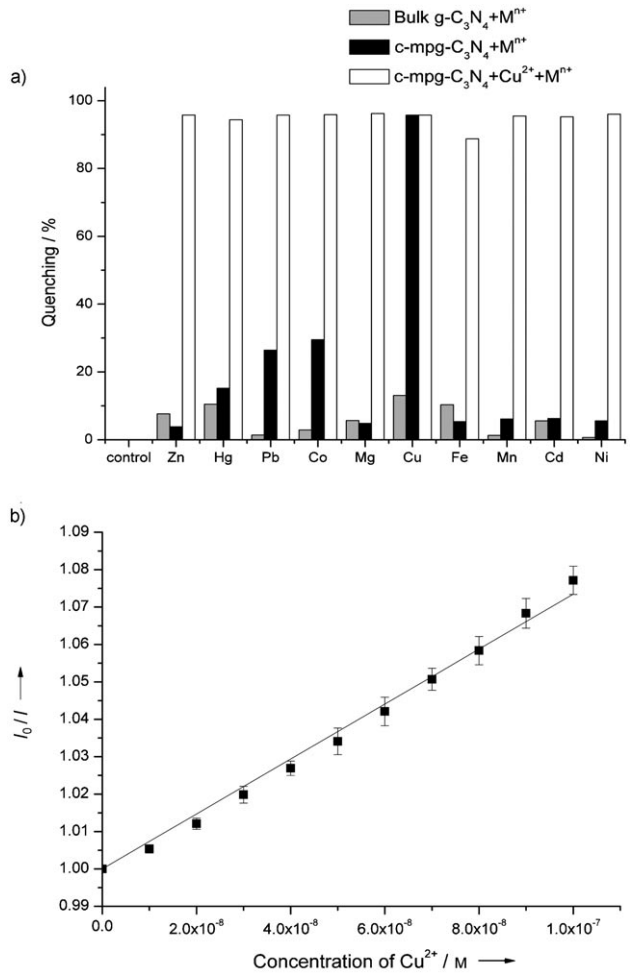

Figure 3. a) Selective PL response of bulk (gray bar) and c-mpg-C_3N_4 (black bar) after treatment of 1 mM metal ion solutions, and interference of 1 mM of other metal ions with 1 mM Cu^{2+} (white bar). b) PL response of c-mpg-C_3N_4 to Cu^{2+} in the concentration range 10–100 nM.

The degree of quenching can be quantitatively described by the Stern–Volmer equation: $I_0/I = 1 + K_{SV}[Q]$.[21] In this equation, I_0 and I are the luminescence intensities in the absence and presence of metal ions, respectively. K_{SV} is the Stern–Volmer constant and $[Q]$ is the molar concentration of metal ion. We used the equation to show the dependency of the luminescence of c-mpg-C_3N_4 on the Cu^{2+} concentration irrespective of its original use for photophysical deactivation processes. A plot of I_0/I versus $[Q]$ for the Cu^{2+}–c-mpg-C_3N_4 system in the concentration range from 10 to 100 nM gives a linear correlation with an R^2 value of 0.992. From this plot, a K_{SV} value of $7.352 \times 10^6\,M^{-1}$ can be calculated and the limit of detection (LOD) in aqueous solution was 12.336 nM (signal to noise ratio is 3) (Figure 3b). The sensitivity of the c-mpg-C_3N_4 system to Cu^{2+} in terms of K_{SV} and LOD is much higher than those of other Cu^{2+}-sensitive systems based on a luminescent metal–organic frameworks ($89.4\,M^{-1}$ [21]), quantum dots ($2.21 \times 10^3\,M^{-1}$, 7.1 μM[22]), and ligand-conjugated inorganic nanoparticles ($26.4 \times 10^3\,M^{-1}$, 380 nM[23]).

Figure S7 (see the Supporting Information) shows the UV/Vis absorption spectra of c-mpg-C_3N_4 before and after addition of Cu^{2+}. c-mpg-C_3N_4 features a typical optical absorption for a semiconductor. A stronger absorption intensity than bulk g-C_3N_4 above $\lambda = 430$ nm due to the enhanced light harvesting ability by the nanostructure.[20] After addition of Cu^{2+}, a new broad absorption band arose at around $\lambda = 700$ nm for c-mpg-C_3N_4, which we attribute to the forbidden d–d transition of Cu^{2+}.[24] The coordinated complex of Cu^{2+} with c-mpg-C_3N_4 is unstable owing to the d^9 configuration of Cu^{2+}; hence, Cu^{2+}–c-mpg-C_3N_4 distorts to circumvent the unstable state. The lowered symmetry of coordinated complex as a result of the distortions removes the orbital degeneracy (Jahn–Teller effect).[25] As a result, the electrons are redistributed within the split d orbitals of Cu^{2+}.

Further investigation into the surface interaction of Cu^{2+} with c-mpg-C_3N_4 was conducted by XPS measurements. Deconvolution of N 1s spectrum of c-mpg-C_3N_4 distinguishes signals with several binding energy (Figure S6a). The pronounced signal centered at 398.5 eV corresponds to C–N=C coordination. The presence of tertiary nitrogen (N–C_3) and amino functions carrying hydrogen (C–N–H or C–N–H_2) was confirmed by the signals observed at 399.6 and 400.7 eV, respectively. It is worth noting that the peak of amino functions surpasses that of tertiary nitrogen by a factor of 4.1. We attribute this to the enhanced surface density of amino/imino functions on c-mpg-C_3N_4. After adsorption of Cu^{2+}, two new signals (399.0 and 401.5 eV) arose at binding energies higher than those of C–N=C and C–N–H, respectively, in the N 1s spectrum of Cu^{2+}-c-mpg-C_3N_4 (Figure S8b). This result can be explained by complex formation between Cu^{2+} and amino/imino functions. Thus, the coordination of N atoms to Cu^{2+} results in a decrease in electron density on the nitrogen atoms and an increase in N 1s binding energy.[26] The contribution of both amino and imino functions on the complex formation is also revealed in the Cu $2p_{3/2}$ spectrum of Cu^{2+}–c-mpg-C_3N_4. Unlike for Cu^{2+}–amine (or phthalocyanine, porphyrin) complexes, the spectrum can be resolved into

two signals at 932.6 and 935.3 eV corresponding to amino- and imino-bound Cu^{2+}, respectively. The former is close to the value reported for amino-bound Cu^{2+} (932.8 eV)[26] and the latter for phthalocyanine-bound Cu^{2+} (935.0 eV).[27]

The quenching effect of Cu^{2+} on the PL intensity of c-mpg-C_3N_4 was also investigated at different coordination conditions, temperature and light (Figure S9 and Table S1). Under dark conditions, K_{SV} increased from $0.0037\times10^6\,M^{-1}$ to $0.0458\times10^6\,M^{-1}$ with increasing temperature from 20 to 37 °C. Moreover, the quenching effect at 20 °C under visible light was approximately 15 times higher than that of dark conditions. From these results, it can be concluded that the higher temperature (presumably the physiological temperature) is preferred to enhance the sensitivity on Cu^{2+} due to the faster diffusion of metal ions to the coordination sites of c-mpg-C_3N_4. Further, it was shown that the electron transfer from c-mpg-C_3N_4 to metal ions can be promoted by visible light and the quenching of c-mpg-C_3N_4 for Cu^{2+} is dominantly induced by the PET from metal ions to c-mpg-C_3N_4.

In conclusion, we have synthesized the "all-in-one" chemosensor, cubic mesoporous ordered graphitic C_3N_4 (c-mpg-C_3N_4) by a nanocasting approach. c-mpg-C_3N_4 is used as an optical sensor for the detection of trace amount of metal ions. The sensor is composed entirely of the functional material, which simultaneously supports a high surface area, efficiently binds to metal ions, and gives a photoelectrical response to the adsorption of the metals. c-mpg-C_3N_4 shows highly selective and sensitive PL response to Cu^{2+} without interference by other metal ions. With fast response time of 5 min for the 90 % of equilibrium PL response, this novel optical sensing system is applicable in the aqueous solution and physiological environment. We believe that it is suitable system for in vivo sensing and imaging by reason of its biocompatibility and high photostability that is kept over several months. For real applications, integration of c-mpg-C_3N_4 into a 96-well plate and loading of analyte solution into the wells should facilitate rapid, simple, and multiple detections without further procedures described herein. Works for sensing and imaging of other ions or biomolecules, and as a vehicle for drug or DNA delivery, are currently underway.

Experimental Section

Synthesis of 3D cubic mesoporous silica KIT-6: 3D cubic mesoporous silica KIT-6 was prepared in 0.5 M HCl solution and 1-butanol.[28] Briefly, P123 (6 g) was dissolved in a solution of HCl (228 g; 37 %). After clear solution was achieved, 1-butanol (6 g) was added, and the solution was stirred for 1 h at 35 °C. TEOS (tetraethyl orthosilicate; 12.9 g) was added, and the mixture was stirred for 1 day in a closed polypropylene bottle under static conditions. Subsequently, the mixture was heated at 130 °C for 1 day. The resulting white precipitate was filtered, dried at 80 °C for 1 day, and then calcined at 550 °C in air for 4 h with a heating rate of 2.3 °C min^{-1}.

Synthesis of bulk g-C_3N_4: Bulk g-C_3N_4 was prepared by direct pyrolysis of melamine in the semiclosed system according to a reported procedure.[29] In a typical synthesis, melamine (20 g, Aldrich, $\geq$ 99 %) was placed in an alumina crucible with a cover and then heated at 550 °C for 4 h with a heating rate of 2.3 °C min^{-1}.

Synthesis of c-mpg-C_3N_4: c-mpg-C_3N_4 was prepared according to a reported procedure.[18] In a typical synthesis, silica template (1 g) was impregnated in an aqueous 7 mM cyanamide solution (1 g), and the mixture was stirred for 1 h, centrifuged, dried in air, and finally calcined under nitrogen for 4 h at a heating rate of 2.3 °C min^{-1}. For better infiltration of cyanamide into the mesopores, the composite was heated at 40 °C for 20 min under vacuum before calcination. To remove the silica template, the resulting bright yellow powder was treated with 4 M NH_4HF_2 for 1 day, filtered, washed with water and ethanol several times, and dried at 50 °C.

Characterization of g-C_3N_4: TEM images were taken with JEOL FB-2100F (HR) at an acceleration voltage of 200 kV, respectively. Characterization by XRD was carried out in reflection mode (Cu Kα radiation) on a Rigaku D/MAX-2500 diffractometer. Elemental analysis was performed three times on different batches of g-C_3N_4s using a Vario EL 3 elemental analyzer manufactured by Elementar. The standard deviation of the atomic weight percentage was lower than 0.36 % for carbon, 0.7 % for nitrogen, and 0.08 % for hydrogen. The adsorption/desorption isotherms of nitrogen at −196 °C were measured using a Micromeritics ASAP 2020. The Brunauer–Emmett–Teller (BET) equation was used to calculate the apparent surface area from adsorption data obtained at P/P_0 between 0.05 and 0.2. The total volume of the micro- and mesopores was calculated from the amount of nitrogen adsorbed at $P/P_0 = 0.99$, assuming that adsorption on the external surface was negligible relative to adsorption in the pores. The pore size distribution was evaluated by BJH method using the adsorption branch. FTIR spectra were collected on a JASCO FT-IR 470 Plus spectrometer with an average of 12 scans with a resolution of 4 cm^{-1} from 4000 cm^{-1} to 600 cm^{-1}. Thermogravimetric analysis (TGA) was carried out using a Dupont 2200 thermal analysis station. Sample was heated from 100 to 1000 °C at a rate of 10 °C min^{-1} under a nitrogen flow of 500 mL min^{-1}. X-ray photoelectron spectroscopy (XPS) spectra were provided by ESCA-LAB250.

Measuring luminescence and absorption of c-mpg-C_3N_4: Metal ion solution (10 mL) in 10 mM tris-HCl buffer at pH 7.4 with various metal nitrates and concentrations was added to g-C_3N_4 (10 mg) in a vial. The metal ion solution with g-C_3N_4 was stirred at room temperature for 30 min and then centrifuged at 4000 rpm for 10 min to remove the metal ion solution from g-C_3N_4. After the supernatant was removed, the separated g-C_3N_4 was resuspended with 10 mL of 10 mM tris-HCl buffer solution. Metal-coordinated g-C_3N_4 (0.2 mL) was sampled its luminescence spectrum was measured. All luminescence spectra were measured by microplate spectrofluorometer (Gemini EM-Molecular Devices, USA). Optical absorbance spectra were examined by ultraviolet diffuse reflectance spectroscopy (V670-Jasco, Japan). Fluorescence images were recorded using inverted fluorescence microscope (Motic AE31-Ted Pella, USA)

Calculation of limit of detection (LOD): The value of LOD was calculated as $LOD = 3\sigma_0/S$, where σ_0 is the standard deviation of PL intensity of c-mpg-C_3N_4 at 455 nm in the absence of metal ion and S is the slope between PL intensity at 455 nm versus metal ion concentration.

Received: August 10, 2010
Published online: ■■ ■■, 2010

Keywords: fluorescence · mesoporous materials · nitrides · sensors · transition metals

[1] a) E. Kroke, M. Schwarz, *Coord. Chem. Rev.* **2004**, *248*, 493 – 532; b) A. Thomas, A. Fischer, F. Goettmann, M. Antonietti, J. O. Muller, R. Schlogl, J. M. Carlsson, *J. Mater. Chem.* **2008**, *18*, 4893 – 4908.

[2] E. Kroke, M. Schwarz, E. Horath-Bordon, P. Kroll, B. Noll, A. D. Norman, *New J. Chem.* **2002**, *26*, 508 – 512.

[3] B. V. Lotsch, M. Doblinger, J. Sehnert, L. Seyfarth, J. Senker, O. Oeckler, W. Schnick, *Chem. Eur. J.* **2007**, *13*, 4969 – 4980.

[4] M. J. Bojdys, J. O. Muller, M. Antonietti, A. Thomas, *Chem. Eur. J.* **2008**, *14*, 8177 – 8182.
[5] a) M. Groenewolt, M. Antonietti, *Adv. Mater.* **2005**, *17*, 1789 – 1792; b) J. S. Zhang, X. F. Chen, K. Takanabe, K. Maeda, K. Domen, J. D. Epping, X. Z. Fu, M. Antonietti, X. C. Wang, *Angew. Chem.* **2010**, *122*, 451 – 454; *Angew. Chem. Int. Ed.* **2010**, *49*, 441 – 444.
[6] X. F. Chen, J. S. Zhang, X. Z. Fu, M. Antonietti, X. C. Wang, *J. Am. Chem. Soc.* **2009**, *131*, 11658 – 11659.
[7] X. C. Wang, X. F. Chen, A. Thomas, X. Z. Fu, M. Antonietti, *Adv. Mater.* **2009**, *21*, 1609 – 1612.
[8] X. C. Wang, K. Maeda, A. Thomas, K. Takanabe, G. Xin, J. M. Carlsson, K. Domen, M. Antonietti, *Nat. Mater.* **2009**, *8*, 76 – 80.
[9] F. Goettmann, A. Fischer, M. Antonietti, A. Thomas, *Angew. Chem.* **2006**, *118*, 4579 – 4583; *Angew. Chem. Int. Ed.* **2006**, *45*, 4467 – 4471.
[10] X. C. Wang, K. Maeda, X. F. Chen, K. Takanabe, K. Domen, Y. D. Hou, X. Z. Fu, M. Antonietti, *J. Am. Chem. Soc.* **2009**, *131*, 1680 – 1681.
[11] E. Palomares, R. Vilar, A. Green, J. R. Durrant, *Adv. Funct. Mater.* **2004**, *14*, 111 – 115.
[12] E. W. Stein, P. S. Grant, H. G. Zhu, M. J. McShane, *Anal. Chem.* **2007**, *79*, 1339 – 1348.
[13] S. J. Lee, J. E. Lee, J. Seo, I. Y. Jeong, S. S. Lee, J. H. Jung, *Adv. Funct. Mater.* **2007**, *17*, 3441 – 3446.
[14] T. Balaji, S. A. El-Safty, H. Matsunaga, T. Hanaoka, F. Mizukami, *Angew. Chem.* **2006**, *118*, 7360 – 7366; *Angew. Chem. Int. Ed.* **2006**, *45*, 7202 – 7208.
[15] M. Ishida, Y. Naruta, F. Tani, *Angew. Chem.* **2010**, *122*, 95 – 98; *Angew. Chem. Int. Ed.* **2010**, *49*, 91 – 94.
[16] S. J. Lee, S. S. Lee, M. S. Lah, J. M. Hong, J. H. Jung, *Chem. Commun.* **2006**, 4539 – 4541.
[17] F. Jiao, A. H. Hill, A. Harrison, A. Berko, A. V. Chadwick, P. G. Bruce, *J. Am. Chem. Soc.* **2008**, *130*, 5262 – 5266.
[18] Y. S. Jun, W. H. Hong, M. Antonietti, A. Thomas, *Adv. Mater.* **2009**, *21*, 4270 – 4274.
[19] Y. C. Zhao, Z. Liu, W. G. Chu, L. Song, Z. X. Zhang, D. L. Yu, Y. J. Tian, S. S. Xie, L. F. Sun, *Adv. Mater.* **2008**, *20*, 1777 – 1781.
[20] X. F. Chen, Y. S. Jun, K. Takanabe, K. Maeda, K. Domen, X. Z. Fu, M. Antonietti, X. C. Wang, *Chem. Mater.* **2009**, *21*, 4093 – 4095.
[21] B. L. Chen, L. B. Wang, Y. Q. Xiao, F. R. Fronczek, M. Xue, Y. J. Cui, G. D. Qian, *Angew. Chem.* **2009**, *121*, 508 – 511; *Angew. Chem. Int. Ed.* **2009**, *48*, 500 – 503.
[22] M. Koneswaran, R. Narayanaswamy, *Sens. Actuators B* **2009**, *139*, 104 – 109.
[23] J. N. Zheng, C. Xiao, Q. Fei, M. Li, B. J. Wang, G. D. Feng, H. M. Yu, Y. F. Huan, Z. G. Song, *Nanotechnology* **2010**, *21*, 1 – 5.
[24] a) J. H. Viles, F. E. Cohen, S. B. Prusiner, D. B. Goodin, P. E. Wright, H. J. Dyson, *Proc. Natl. Acad. Sci. USA* **1999**, *96*, 2042 – 2047; b) M. G. Savelieff, Y. Lu, *Inorg. Chim. Acta* **2008**, *361*, 1087 – 1094.
[25] K. De Wael, A. Adriaens, *Talanta* **2008**, *74*, 1562 – 1567.
[26] S. B. Deng, R. B. Bai, J. P. Chen, *Langmuir* **2003**, *19*, 5058 – 5064.
[27] B. Adolphi, O. Berger, W. J. Fischer, *Appl. Surf. Sci.* **2001**, *179*, 102 – 108.
[28] F. Kleitz, S. H. Choi, R. Ryoo, *Chem. Commun.* **2003**, 2136 – 2137.
[29] S. C. Yan, Z. S. Li, Z. G. Zou, *Langmuir* **2009**, *25*, 10397 – 10401.

Communications

Chemosensors

E. Z. Lee, Y.-S. Jun,* W. H. Hong,*
A. Thomas, M. M. Jin ——— ■■■■–■■■■

Cubic Mesoporous Graphitic Carbon(IV) Nitride: An All-in-One Chemosensor for Selective Optical Sensing of Metal Ions

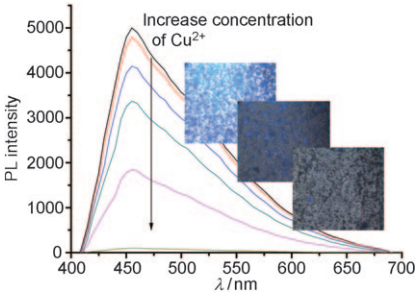

I can Cu: Cubic mesoporous graphitic carbon nitride (c-mpg-C_3N_4) is an all-in-one chemosensor that plays the roles of ligand, fluorophore, and supporting material, enables the simple detection of metal ions, and is highly selective and sensitive to Cu^{2+}.